Jurnal Rekayasa Mesin
p-ISSN: 1411-6863, e-ISSN: 2540-7678
Vol. 18, No. 3, Desember **2023**, hal. 409-418

Experimental and Numerical Study of Shock Absorber Characterization and The Implication on The Dynamics of Half Vehicle Suspension System Model

Avicenna An-Nizhami[1*], Nanang Budi Sriyanto[1], Bambang Sumiyarso[1], Showi Nailul Ulum[1], Elfrida Rizky Riadini[2] dan Ignatius Gunawan Widodo[1]
[1]Mechanical Engineering Department, Politeknik Negeri Semarang,
Jl. Prof. Sudarto, Kota Semarang, 50275
[2]Mechanical Engineering Department, Universitas Gadjah Mada,
Bulaksumur, Kabupaten Sleman, Daerah Istimewa Yogyakarta, 55281

*E-mail: avicenna@polines.ac.id

Diajukan: 02-10-2023; Direvisi: 08-12-2023; Dipublikasi: 22-12-2023

Abstract

This study aimed to characterized shock absorber damping for passenger comfort. The riding comfort of the vehicle has direct correlation to the damping characteristic of the shock absorber of the suspension system. Two different shock absorbers were experimentally evaluated, and their damping characteristics were integrated into a half-car model to study the vehicle's dynamic response to harmonic road disturbances. The investigation involved numerical simulations of the half-car model subjected to harmonic road disturbances, represented by a set of ordinary differential equations solved using the Dormand-Prince method. Experimental data yielded average damping forces of 502.77 N for shock-absorber #1 and 192.03 N for shock-absorber #2. Calculations resulted in damping coefficients of 3888.57 N·s/m for shock-absorber #1 and 1397.85 N·s/m for shock-absorber #2, with corresponding damping ratios of 0.29 and 0.105. These damping ratios generally aligned with typical values for passenger car shock absorbers, except for shock-absorber #2, which deviated from the expected range. The study found that at 60 km/h and 90 km/h, shock-absorber #1 with ζ=0.29 exhibited superior performance in reducing displacement amplitude compared to shock-absorber #2 at ζ=0.105. However, at 120 km/h, both shock-absorbers displayed similar responses, with shock-absorber #1 slightly surpassing shock-absorber #2 in displacement amplitude.

Keywords: damping ratio; displacement; ride comfort; shock absorber; vehicle dynamics

Abstrak

Penelitian ini bertujuan untuk mengkarakterisasi peredam getaran untuk kenyamanan penumpang. Kenyamanan berkendara memiliki hubungan langsung dengan karakteristik redaman dari peredam getaran pada sistem suspensi. Dua peredam getaran yang berbeda dievaluasi secara eksperimental, dan karakteristik redaman mereka diintegrasikan ke dalam model half car untuk mengkaji respon dinamis kendaraan terhadap eksitasi harmonik pada permukaan jalan. Penelitian ini melibatkan simulasi numerik dari model half car yang terkena eksitasi harmonik, yang diwakili oleh persamaan diferensial yang dipecahkan menggunakan metode Dormand-Prince. Data eksperimental menghasilkan gaya redaman rata-rata sebesar 502,77 N untuk peredam getaran #1 dan 192,03 N untuk peredam getaran #2. Perhitungan menghasilkan koefisien redaman sebesar 3888,57 N·s/m untuk peredam getaran #1 dan 1397,85 N·s/m untuk peredam getaran #2, dengan rasio redaman 0,29 dan 0,105. Rasio redaman hasil pengujian untuk kedua peredam getaran sesuai dengan nilai tipikal untuk peredam getaran mobil penumpang, kecuali peredam getaran #2 yang sedikit melebihi rentang nilai yang diharapkan. Pada hasil studi numerik ditemukan bahwa pada kecepatan 60 km/jam dan 90 km/jam, peredam getaran #1 dengan ζ=0,29 menunjukkan kinerja yang lebih baik dalam mengurangi amplitudo perpindahan dibandingkan dengan peredam getaran #2 pada ζ=0,105. Namun, pada kecepatan 120 km/jam, kedua peredam getaran menunjukkan respons yang hampir serupa, dengan peredam getaran #1 sedikit melebihi peredam getaran #2 dalam amplitudo perpindahan.

Kata kunci: *rasio redaman; perpindahan; kenyamanan berkendara; peredam getaran; dinamika kendaraan*

1. Introduction

The dynamic responsiveness and comfort of mechanical systems and automobiles both depend critically on the damping properties of the shock absorbers. How well the shock absorbers disperse energy from outside disturbances depends on these features. The disturbance caused by vehicle operation such as acceleration, braking and cornering. In terms of dynamics response, properly adjusted damping is essential for eliminating oscillations, improving handling, minimizing body roll while cornering, and guaranteeing steady traction and grip, all of which are essential for safety

and performance. Additionally, damping reduces the force of jolts caused by road imperfections, protecting passengers and cargo from harm. In terms of comfort, damping is crucial for minimizing vibrations, noise transmission, and the roughness of the ride. It is crucial for passenger cars where comfort is a major goal. In the end, damping qualities have a substantial influence on how good, safe, and satisfying the ride or operation is overall. The optimization of a suspension system through the precise calibration of damping coefficients for shock absorbers and the tuning of spring stiffness holds the potential to mitigate wear and extend the operational longevity of vehicles traversing specific road profiles.

An-Nizhami et al. [1] delved into enhancing the comfort and dynamic response of the vehicle's sprung mass through the application of a semi-active suspension system utilizing PID controller on the half-car model. Their investigation revealed a notable enhancement in the dynamic response of the sprung mass, particularly when exposed to higher-frequency disturbances. In a related study, Silveira et al. [2] examined the efficacy of symmetrical (linear) versus asymmetrical (nonlinear) shock absorbers in passenger vehicles, considering diverse road inputs, severity levels, asymmetry ratios, and vehicle velocities. Their findings underscored that an asymmetrical system characterized by nonlinear properties delivered a smoother and more gradual performance in both vertical and angular movements.

One approach to ameliorating comfort and handling entails the integration of an active system, encompassing closed-loop system control and active actuators [3]–[8] and active shock absorber which can be varied, the so-called semi-active suspension system [1], [9], [10]. However, it is worth noting that one of the limitations associated with active suspension systems is the substantial cost incurred in implementing the entire suspension system, encompassing the control apparatus and actuators. Furthermore, the amplitude and frequency of vibrations play a pivotal role in influencing passenger comfort levels, with these factors intricately determined by the characteristics of the road profile.

In order to study the dynamic response of the vehicle, half car or half vehicle suspension system model often used as a tool to study the vertical movement and pitching of the vehicle. Xue et al. [11] introduced a method for robust road profile estimation and vehicle parameter identification using smartphone data, employing a half-car model. Zhang et al. [12] investigated regenerative shock absorbers integrated with quarter, half, and full vehicle suspension system models, revealing that the quarter model exhibits inaccuracies in low-frequency power output and is limited to specific driving cycles, while the half and full models demonstrate accurate power output across various frequency ranges, vehicle speeds, and road classifications, particularly when neglecting transverse road profiles. Wu et al. [13] introduced a novel controller design for half-car magneto-rheological suspension systems, employing a piecewise approximation model to transform nonlinear constraints into piecewise constant constraints, and utilizing a piecewise affine control law with linear-matrix-inequality optimization to achieve pitch and heave response attenuation. Gandhi et al. [14] employed a half-car active suspension model with 4 Degrees of Freedom (4 DOF) and evaluates Proportional Integral Derivative, Linear Quadratic Regulator, Fuzzy, and Adaptive Neuro Fuzzy Inference System (ANFIS) controllers.

In order to find an optimal damping characteristic of the shock absorber to improve drive comfort for the passenger, in this study two different shock absorbers are investigated experimentally to find the damping characteristics and then implement the damping value to the half car model to investigate the dynamics response of a vehicle undergoing harmonic road disturbances. By exploring and comprehending the behavior of shock absorbers, this study contributes to advancements in vehicle suspension design, potentially leading to improved vehicle performance, comfort, and safety.

The paper is organized into sections. The first section is an introduction explaining the background of the study and literature review. The second section is methodology, this section describes the experimental setup and the implementation of experimental analysis on mathematical model of the half car. The third section presents the results and discusses the analysis of the results. The fourth section is the conclusion of the study.

2. Material and Methodology

The experiments are conducted with the primary objective of determining the damping forces exhibited by two distinct shock absorbers. These experimental trials were carried out not just once but repeated a total of three times to ensure accuracy and to subsequently compute the average value of the damping force for each shock absorber. Figure 1 shows the shock absorber testing machine, a specialized piece of equipment designed for the purpose of subjecting shock absorber specimens to a testing, the machine also includes the digital force sensor to measure the damping force. The force assessment was conducted utilizing a push-pull digital force gauge, with its peak load capacity at 9800 N. This machine, serving as a critical component in our experimental setup, has been configured to examine the damping properties of the shock absorbers under a given scenario. Moreover, alongside the testing machine, the shock absorber specimen itself is displayed, providing a representation of the component being evaluated in our testing procedures.

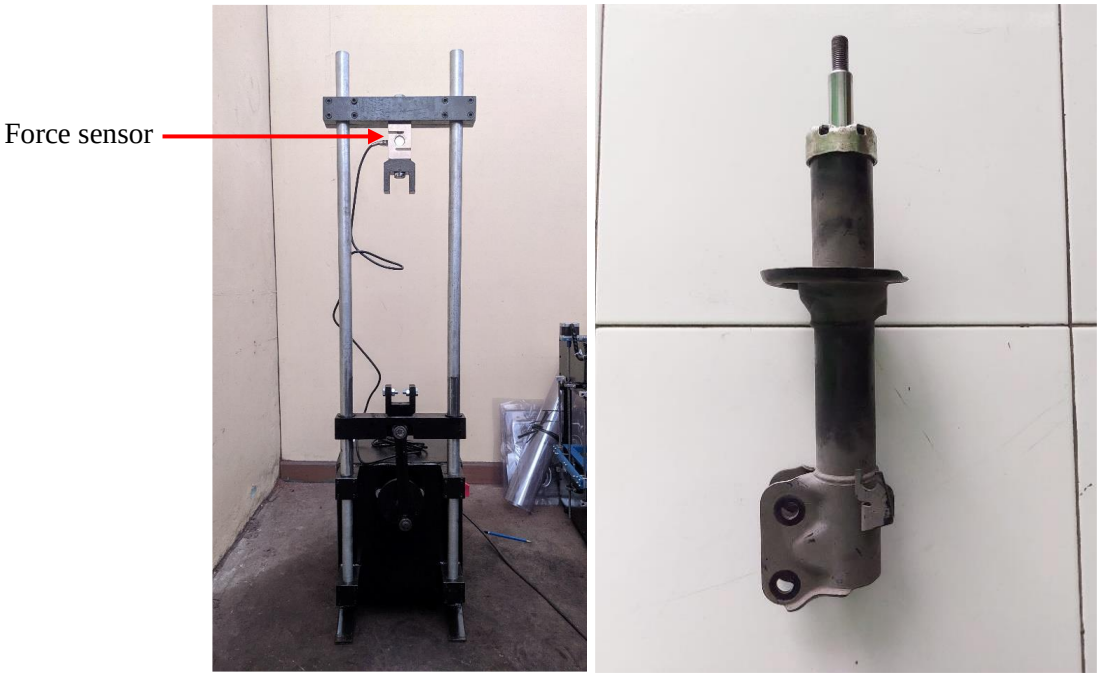

Figure 1. Shock absorber testing machine and a shock absorber specimen

Figure 2 depicts the half car model, a schematic representation of a vehicle's structure and suspension system. In this depiction, the suspension system was conceptualized as a combination of a spring and damper. Within this framework, M symbolizes the mass of the vehicle, y characterizes the displacement of the vehicle mass, while k and c denote the parameters signifying suspension spring stiffness and shock absorber damping coefficient, respectively. The vibration phenomena within this system were mathematically represented by ordinary differential equations (ODEs), as shown in Eqs. $(1) - (5)$. These ODEs served as a mathematical description of the dynamic behaviour of the vehicle in the vertical plane, encapsulating key aspects such as displacement, velocity, and acceleration in response to harmonic disturbances.

Table 1. Symbol and symbol description used in this study [1]

Symbol	Symbol description
M	Sprung mass [kg]

Symbol	Symbol description
m	Unsprung mass [kg]
Z	Displacement of sprung/unsprung mass [m]
CG	Center of gravity
θ	Angular displacement of sprung mass [rad]
l	Wheel and *CG* distance [m]
k	Suspension spring stiffness coefficient [N/m]
C	Suspension shock absorber damping coefficient [N.s/m]
w	Road disturbance [m]
Cc	Critical damping [N.s/m]
ζ	Damping ratio

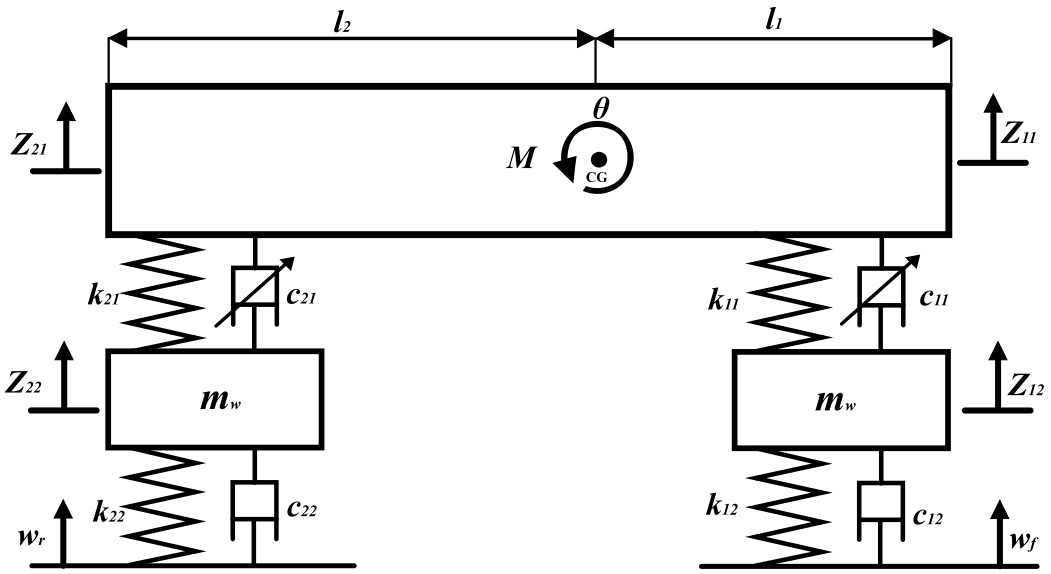

Figure 2. Half car model used in the current study [1]

$$I\frac{d^2\theta}{dt^2} = k_{11}(z_{12} - z_{11} - \theta l_1)l_1 + c_{11}\left(\frac{dz_{12}}{dt} - \frac{dz_{11}}{dt} - \frac{d\theta}{dt}l_1\right)l_1 \quad - k_{21}(z_{22} - z_{21} - \theta l_2)l_2 \quad (1)$$

$$-c_{21}\left(\frac{dz_{22}}{dt} - \frac{dz_{21}}{dt} - \frac{d\theta}{dt}l_2\right)l_2$$

$$M\frac{d^2z_{11}}{dt^2} = k_{11}(z_{12} - z_{11} - \theta l_1) + c_{11}\left(\frac{dz_{12}}{dt} - \frac{dz_{11}}{dt} - \frac{d\theta}{dt}l_1\right) \quad (2)$$

$$M\frac{d^2z_{12}}{dt^2} = k_{12}(w_f - z_{12}) + c_{12}\left(\frac{dw_f}{dt} - \frac{dz_{12}}{dt}\right) - k_{11}(z_{12} - z_{11} - \theta l_1) - c_{11}\left(\frac{dz_{12}}{dt} - \frac{dz_{11}}{dt} - \frac{d\theta}{dt}l_1\right) \quad (3)$$

$$M\ \frac{d^2z_{21}}{dt^2} = k_{21}(z_{22} - z_{21} - \theta l_2) + c_{21}\left(\frac{dz_{22}}{dt} - \frac{dz_{21}}{dt} - \frac{d\theta}{dt}l_2\right) \quad (4)$$

$$M\frac{d^2z_{22}}{dt^2} = k_{22}(w_r - z_{22}) + c_{12}\left(\frac{dw_r}{dt} - \frac{dz_{22}}{dt}\right) - k_{21}(z_{22} - z_{21} - \theta l_2) - c_{21}\left(\frac{dz_{22}}{dt} - \frac{dz_{21}}{dt} - \frac{d\theta}{dt}l_2\right) \quad (5)$$

The process of modelling involves the solution of ODEs that were tailored to the given scenario. These differential equations were subsequently subjected to a temporal integration, and this integration task was executed through the utilization of the Dormand-Prince method [15]. The Dormand-Prince method represents a numerical method harnessed for the resolution of ordinary differential equations. It employs a set of six function evaluations within its computation, with levels of accuracy corresponding to the fourth and fifth orders denoted as Eqs. (6)-(12). In the validation case, a scenario titled as 'Vehicle Moving on a Rough Road' [16] have been performed on the previous study [1].

$$k_1 = \Delta t\, f(t, \dot{y}) \quad (6)$$

$$k_2 = \Delta t\, f\left(t + \frac{1}{5}\Delta t, \dot{y} + \frac{1}{5}k_1\right) \quad (7)$$

$$k_3 = \Delta t\, f\left(t + \frac{3}{10}\Delta t, \dot{y} + \frac{3}{40}k_1 + \frac{9}{40}k_2\right) \quad (8)$$

$$k_4 = \Delta t\, f\left(t + \frac{4}{5}\Delta t, \dot{y} + \frac{44}{45}k_1 - \frac{56}{15}k_2 + \frac{32}{9}k_3\right) \quad (9)$$

$$k_5 = \Delta t\, f\left(t + \frac{8}{9}\Delta t, \dot{y} + \frac{19372}{6561}k_1 - \frac{25360}{2187}k_2 + \frac{64448}{6561}k_3 - \frac{212}{729}k_4\right) \quad (10)$$

$$k_6 = \Delta t\, f\left(t + \Delta t, \dot{y} + \frac{9017}{3168}k_1 - \frac{355}{33}k_2 + \frac{46732}{5247}k_3 + \frac{49}{176}k_4 - \frac{5103}{18656}k_5\right) \quad (11)$$

$$y_{n+1} = y_n + \frac{35}{384}k_1 + \frac{500}{1113}k_3 + \frac{125}{192}k_4 - \frac{2187}{6784}k_5 + \frac{11}{84}k_6 \quad (12)$$

3. Results and discussion

The data presented in Table 2 pertains to an experimental examination involving two distinct shock absorber specimens. These recorded values explicitly represent the characteristic of damping force magnitude. It is an essential parameter used for the determination of the damping coefficient of the shock absorbers. In this pursuit, it is important to underscore that, out of the three available data points, in this study the mathematical average is to be implemented in the calculation of the damping coefficient.

Table 2. Experimental data of damping force from two different shock-absorbers

Experiment	Shock Absorber #1	Shock Absorber #2
$\mathbf{1}^{st}$ experiment	544.4 N	187 N
$\mathbf{2}^{nd}$ experiment	506.4 N	195.7 N
$\mathbf{3}^{rd}$ experiment	457.5 N	193.4 N

The experiment has resulted in a pair of average damping force values, standing at 502.77 N and 192.03 N, respectively, attributed to shock-absorber #1 and #2. These quantifications serve as numerical inputs for the subsequent

derivation of the damping coefficient. The calculation of said damping coefficient was performed by utilizing the mathematical expression denoted in Eq. 13. The calculated results of the damping coefficient are 3888.57 N.s/m and 1397.85 N.s/m for shock-absorber #1 and #2 respectively.

$$C = \frac{F_D}{dz/dt} \tag{13}$$

Upon the determination of the damping coefficient through our analytical procedure, the subsequent step entails the damping ratio (ζ) for each of the two distinct shock-absorbers under scrutiny. It is imperative to initiate with the calculation of the critical damping, which is established utilizing the formula denoted in Eq. 14. Subsequently, the damping ratio is ascertained through the utilization of Eq. 15 and Table 3. This methodical approach ultimately yields calculated damping ratios of 0.29 and 0.105 for shock-absorber #1 and #2, respectively, underscoring the damping characteristics inherent to each specimen.

$$Cc = 2M\sqrt{\frac{k}{M}} \tag{14}$$

$$\zeta = \frac{C}{Cc} \tag{15}$$

Table 3. Parameters used in the numerical study

Symbol	Value
M	835 [kg]
m	50 [kg]
k	52,250 [N/m]
$\boldsymbol{C_1}$	3888.57 [N.s/m]
$\boldsymbol{C_2}$	1397.85 [N.s/m]
k_w	120.000 [N/m]
c_w	100 [N.s/m]
l_1	1,5 [m]
l_2	1,8 [m]
A	0,05 [m]

The data acquired according to categories devised by Calvo *et al.* [17] falls within the spectrum of typical damping ratios for passenger car shock-absorbers, specifically for shock-absorber #1. This range is typically within the interval of 0.2 to 0.25. In contrast, the damping ratio value obtained for shock-absorber #2 exceeds the confines of this range, thus signifying that its damping characteristics deviate from what is conventionally observed in passenger car suspension systems.

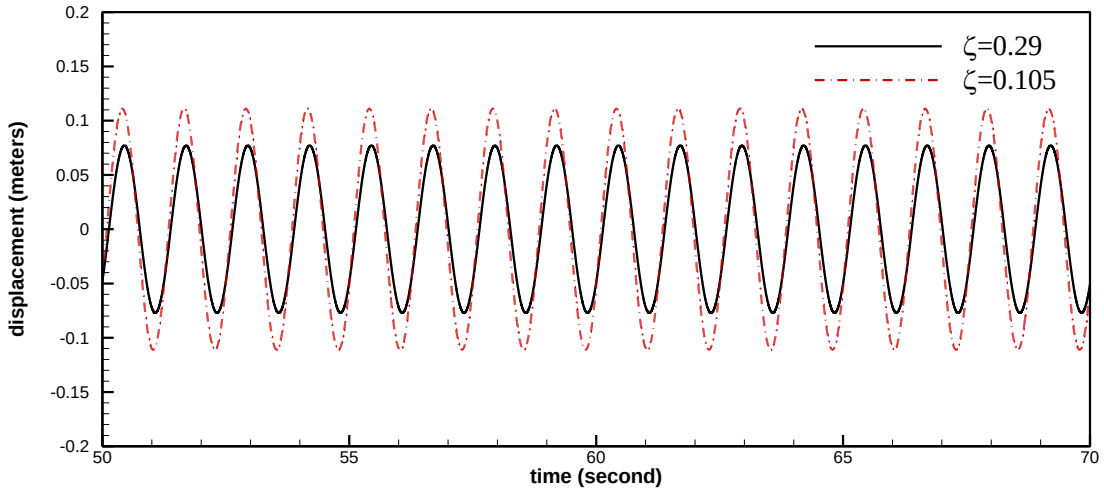

Figure 3. Displacement of the vehicle body in z-axis direction at the speed of 60 km/h

A computational investigation involving the analysis of a half-car model subjected to harmonic road disturbances was conducted across a range of velocities, namely 60 [km/h], 90 [km/h], and 120 [km/h]. The findings have been rendered in the form of illustrative representations, as showcased in Figures 3, 4, and 5. Upon closer look, it becomes patently clear that, at the velocity of 60 [km/h], the displacement response corresponding to a damping coefficient (ζ) of 0.29 exhibits a superior performance. This superiority is markedly evidenced by the diminished amplitude in the displacement response, in stark contrast to the response for shock-absorber at $\zeta = 0.105$. These outcomes imply that shock-absorber #1, characterized by a damping coefficient of $\zeta = 0.29$, possesses an enhanced capacity for the dissipation of kinetic energy when compared to its counterpart, shock-absorber #2.

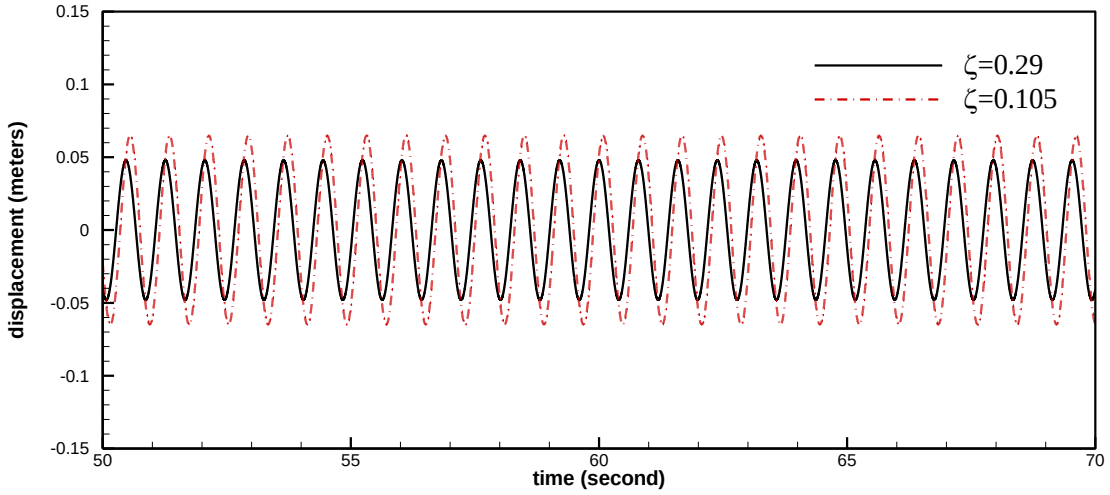

Figure 4. Displacement of the vehicle body in z-axis direction at the speed of 90 km/h

A similar pattern of behavior is also discernible when the vehicle operates at the velocity of 90 [km/h], albeit with a discrepancy in amplitude. In this context, the discrepancy in amplitude, while noticeable, does not exhibit the same degree of significance as observed at the 60 km/h speed setting.

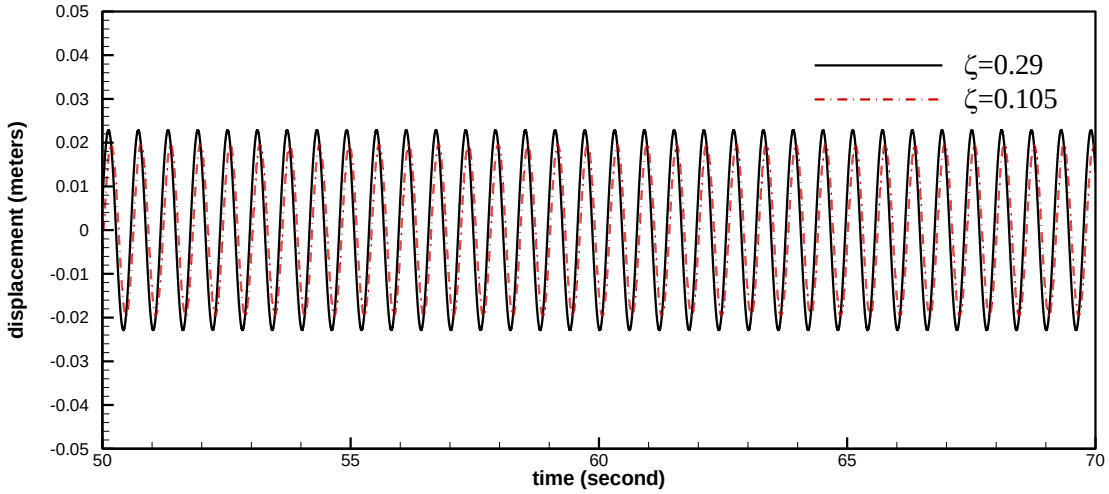

Figure 5. Displacement of the vehicle body in z-axis direction at the speed of 120 km/h

Conversely, when the vehicle operates at the elevated velocity of 120 km/h, a departure from the earlier observed trend emerges. At this speed, the response characteristics for both shock-absorbers manifest nearly identical behaviors. There is particular anomaly witnessed at the 120 km/h speed regime, wherein the amplitude of displacement for shock-absorber #1, with a damping coefficient of ζ=0.29, slightly surpasses that of shock-absorber #2.

4. Conclusion

The experimental data provided average damping forces of 502.77 N for shock-absorber #1 and 192.03 N for shock-absorber #2. These values were used to calculate damping coefficients, resulting in 3888.57 N·s/m for shock-absorber #1 and 1397.85 N·s/m for shock-absorber #2. Subsequently, damping ratios were computed as 0.29 for shock-absorber #1 and 0.105 for shock-absorber #2. These findings align with typical damping ratios for passenger car shock-absorbers, except for shock-absorber #2, which deviates from the norm. The study analyzed a half-car model under harmonic road disturbances at speeds of 60 km/h, 90 km/h, and 120 km/h. At 60 km/h, shock-absorber #1 with ζ=0.29 showed superior performance in the displacement amplitude compared to shock-absorber #2 at ζ=0.105. A similar trend was observed at 90 km/h, though with less amplitude difference. However, at 120 km/h, both shock-absorbers exhibited similar responses, and shock-absorber #1 slightly exceeded shock-absorber #2 in displacement amplitude.

The constraint inherent in this investigation lies in the inability of testing apparatus to characterize the nonlinear attributes of the shock absorber, consequently, our forthcoming research will be directed towards characterizing the non-linear features of the shock absorber, encompassing not only conventional shock absorbers but also those with regenerative function.

Acknowledgment

The authors would like to express their sincere gratitude to Politeknik Negeri Semarang for their financial support through the Penelitian Pratama scheme. This support was instrumental in conducting the research presented in this paper.

References

[1] Avicenna An-Nizhami, Nanang. Apriandi, Padang Yanuar, and Wahyu Isti Nugroho, Pemodelan sistem suspensi pasif dan semi aktif regeneratif dengan model half car dan eksitasi harmonik. Jurnal Rekayasa Mesin. 2022 Agustus; 17 (02): pp. 297-306.

[2] M. Silveira, B. R. Pontes, and J. M. Balthazar, Use of nonlinear asymmetrical shock absorber to improve comfort on passenger vehicles. J Sound Vib. 2014 March; 333(07): pp. 2114–2129.

[3] Q. H. Nguyen, S. B. Choi, and Y. G. Park, An analytical approach to optimally design of electrorheological fluid damper for vehicle suspension system. Meccanica. 2012 October; 47 (07): pp. 1633–1647.

[4] Jimoh O. Pedro, Shakile M. S. Nhlapo, and Lindokuhle J. Mpanza, Model predictive control of half-car active suspension systems using particle swarm optimisation. IFAC-PapersOnLine. 2020 January; 53 (2): pp. 14438–14443.

[5] G. Wang, C. Chen, and S. Yu, Optimization and static output-feedback control for half-car active suspensions with constrained information. J Sound Vib. 2016 September; 378: pp. 1–13.

[6] C. Hua, J. Chen, Y. Li, and L. Li, Adaptive prescribed performance control of half-car active suspension system with unknown dead-zone input. Mech Syst Signal Process. 2018 October; 111: pp. 135–148.

[7] C. Onat, I. B. Kucukdemiral, S. Sivrioglu, I. Yuksek, and G. Cansever, LPV gain-scheduling controller design for a non-linear quarter-vehicle active suspension system. Transactions of the Institute of Measurement & Control. 2009; 31 (1): pp. 71–95.

[8] N. Zulkarnain, H. Zamzuri, and S. A. Mazlan, Ride and handling analysis for an active anti-roll bar: case study on composite nonlinear control strategy. International Journal of Automotive and Mechanical Engineering. 2014 March; 10: pp. 2122–2242.

[9] K. M. M. Rathai, M. Alamir, and O. Sename, GPU based stochastic parameterized NMPC scheme for control of semi-active suspension system for half car vehicle. IFAC-PapersOnLine. 2020 January; 53(2): pp. 14369–14374.

[10] J. Emura, S. Kakizaki, F. Yamaoka, and M. Nakamura, Development of the semi-active suspension system based on the sky-hook damper theory. SAE Transactions. 1994; 103: pp. 1110–1119.

[11] K. Xue, T. Nagayama, and B. Zhao, Road profile estimation and half-car model identification through the automated processing of smartphone data. Mech Syst Signal Process. 2020 August; 142: p. 106722.

[12] R. Zhang, L. Zhao, X. Qiu, H. Zhang, and X. Wang, A comprehensive comparison of the vehicle vibration energy harvesting abilities of the regenerative shock absorbers predicted by the quarter, half and full vehicle suspension system models. Appl Energy. 2020 August; 272: p. 115180.

[13] J. Wu and Z. Liu, Piecewise affine H∞ control of half-car magneto-rheological suspension systems. IFAC-PapersOnLine. 2018 January; 51(31): pp. 967–972.

[14] P. Gandhi, S. Adarsh, and K. I. Ramachandran, Performance analysis of half car suspension model with 4 DOF using PID, LQR, FUZZY and ANFIS controllers. Procedia Comput Sci. 2017 January; 115: pp. 2–13.

[15] J. R. Dormand and P. J. Prince, A family of embedded Runge-Kutta formulae. J Comput Appl Math. 1980 March; 6(1): pp. 19–26.

[16] S. S. Rao, Mechanical vibrations. Prentice Hall, 2011.

[17] J. A. Calvo, V. Díaz, and J. L. San Román, Establishing inspection criteria to verify the dynamic behaviour of the vehicle suspension system by a platform vibrating test bench. International Journal of Vehicle Design. 2005; 38(4): pp. 290–306.